Influence of stores on the flow inside UCAV weapon bays

S. J. Lawson

CFD Laboratory, Department of Engineering
University of Liverpool
Liverpool, UK

G. N. Barakos
G.Barakos@liverpool.ac.uk

ABSTRACT

Detached-eddy simulations for the 1303 UCAV geometry are undertaken aiming to investigate the flow physics of the interaction of a store with the flow inside a UCAV weapons bay. Advanced multi-block topologies had to be used to properly represent the planform of the UCAV and all the details of the weapon bay, including doors and hinges, while sliding meshes were needed to insert the store into the UCAV configuration. Results with an empty bay were encouraging for such complex configurations. Flow visualisation revealed the added turbulent content due to the door leading edges and hinges. The addition of a store in between the doors had little effect close to the front wall of the bay. However averaged flow-fields showed that the proximity of the shear layer to the apex of the store deflected it downwards into the bay and restricted its growth.

1.0 INTRODUCTION

Internal carriage of stores in weapon bays of uninhabited combat air vehicles (UCAVS) has been a major issue and much research has been performed in order to fully understand the complex aerodynamics and aero-acoustics associated with it. Since the pioneering works in the 1950s and 1960s[1-3], numerous experimental investigations have been performed on idealised geometries as well as realistic aircraft configurations. Numerical studies, however, have been largely limited to idealised geometries. Early studies of cavity flows began with utilising the unsteady Reynolds-averaged Navier-Stokes (URANS) equations. It soon became apparent that URANS was not capable of predicting the effect of the range of turbulent scales that exist in cavity flows. Therefore CFD studies moved towards large eddy simulation (LES)[4,5] and detached eddy simulation (DES)[5-7], which provided much better agreement with experimental data.

Paper No. 3572. Manuscript received 13 May 2010, first revision received 27 February 2011, second revision received 30 June 2011, accepted 13 July 2011.

https://doi.org/10.1017/S0001924000006709 Published online by Cambridge University Press



Figure 1. The 1303 UCAV Model installed inside the QinetiQ five-metre wind-tunnel test section[14].

From an aerodynamics point of view, UCAVs present new challenges. One of these may be the presence of exposed weapon bays. Wong *et al*[8] presented results from the Technical Cooperation Program (TTCP) studying a design designated 1303 UCAV, which resulted in experimental and numerical data. These results showed that the Reynolds-averaged Navier-Stokes equations (coupled with various turbulence closures) gave a reasonable overall prediction for the external flow without a weapon bay at modest angles of attack.

When a weapon bay was added to the 1303 UCAV geometry, results from a DES computation[9-12] were compared to experiments by Hill and Lawson[13]. A small over-prediction in the overall sound-pressure level (OASPL) was seen all along the weapon bay floor, which had a maximum of 3dB at around the mid-point of the bay. The aim of the current paper is to obtain a set of numerical results for the 1303 UCAV with a store inserted in the weapon bay.

It is the authors' view that this is the first time that such calculations have been performed and compared against experimental data.

2.0 EXPERIMENTAL DATA

2.1 Setup and data acquisition

Three data sets were available for the 1303 UCAV model. Low speed experiments, performed by Bruce and Mundell[14] at the QinetiQ 5 meter low-speed wind tunnel (Fig. 1), were the main focus of the TTCP study[8]. High Mach number tests on the external flow[15] and investigations into the influence of a store on the flow within the bay[13] were also performed. The UCAV had a wing span of 1·5 metres and a leading-edge sweep of 47°. The air intake was faired over in the model and the rear fuselage was modified to accommodate a sting mounting. Also, the model had no movable control surfaces.

The weapon bay had a length of approximately 0·25 metres and a depth of 0·046 metres, giving an L/D ratio of 5·45. The width was approximately 0·06 metres, yielding a W/D ratio of 1·32. These dimensions are only approximate as the opening of the bay followed the lower surface of the UCAV, which meant that the cross-section was not orthogonal. In fact, the bay was not symmetric about any axis line. The store studied in conjuction with the weapon bay was of a generic type.

Experiments were performed at Mach 0·85 and Reynolds number of 7·34million based on the mean aerodynamic chord (MAC) of the UCAV. For the initial tests, the UCAV model was positioned at approximately zero incidence, sideslip and yaw to the oncoming flow. Additional tests

https://doi.org/10.1017/S0001924000006709 Published online by Cambridge University Press

Table 1
Locations of the store in the 1303 UCAV experiments[13]

Number	Store Location	y (mm)	y/L
1	Far field (FF)	172·32	0·684
2	Between bay doors (DC)	19·95	0·079
3	Bay exit plane (SL)	0·0	0·0
4	Carriage location (CL)	–30·47	–0·121

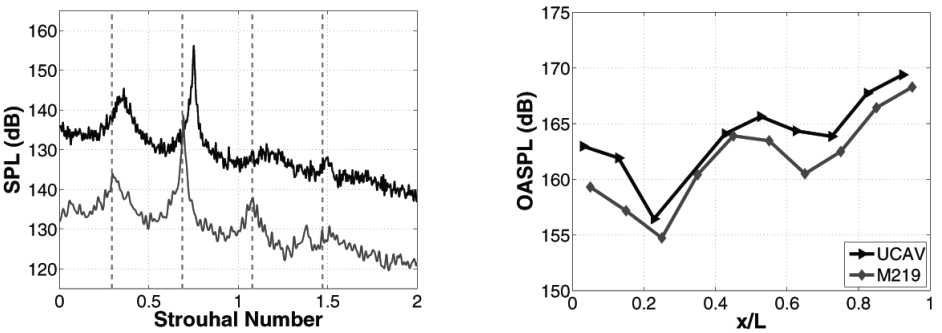


Figure 2. PSD at the rear of the weapon bay and OASPL along the bay floor for the experimental UCAV, and M219 clean cavity with doors. PSD Plot is presented in terms of SPL and for clarity, the curves in the PSD plot are separated by introducing offsets. Vertical dashed lines on PSD represent the frequencies of Rossiter's Modes[3].

at angles of attack of –4° and 4°, and sideslip angles of –5° and 5° were performed, but these were not considered in the current study. Tests were performed with the store statically placed in four different locations: inside the bay, on the exit plane (on the bay shear layer), in the middle of the bay doors and in the far-field. The exact location of the store in the normal direction is summarised in Table 1. Note that no data is available without the store, instead the store was traversed a large distance away from the bay opening.

The weapon bay floor was instrumented with ten dynamic pressure transducers, which were located off the centreline of the bay. Further pressure taps were placed on the fore and aft walls of the bay. Also, numerous static pressure taps were located inside the bay, on the walls, the doors and on the store. The store was also connected to a force-balance to measure time-averaged effects on the store itself.

2.2 Unsteady pressure data

Unsteady pressure data for the empty UCAV weapon bay (case number 1 in Table 1) and the ideal M219 cavity data with doors attached[16] is compared to show the similarities in frequency content of the flow for the realistic UCAV geometry and idealistic cavity geometry. The power spectral density (PSD) and the OASPL for the two cases are presented in Fig. 2. The PSD is presented in terms of the Strouhal number because of the different geometry and test conditions, and an offset has been introduced in the pilot, to clearly show the two PSD curves. The tones occurred at lower Strouhal numbers in the M219 cavity case and the third mode was more

https://doi.org/10.1017/S0001924000006709 Published online by Cambridge University Press

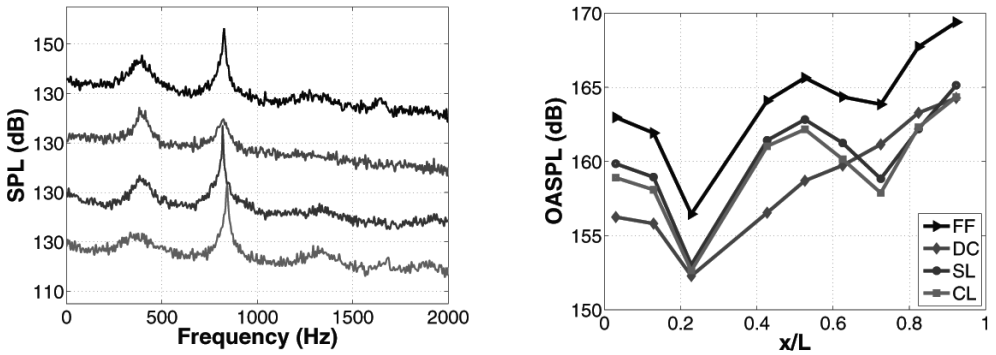


Figure 3, PSD at the rear of the weapon bay and OASPL along the bay floor for the experimental UCAV with a store positioned at the far field (FF) , the centre of the doors (DC), the shear layer (SL) and the carriage location (CL). PSD plot is presented in terms of SPL and the curves are separated for clarity.

evident. The amplitude of the first mode for the two cases was similar, although the second and third modes were higher in the M219 case. However, the broadband noise had similar levels. The OASPL revealed that generally, the UCAV had higher levels along the cavity length, with differences being between 1 and 4dB.

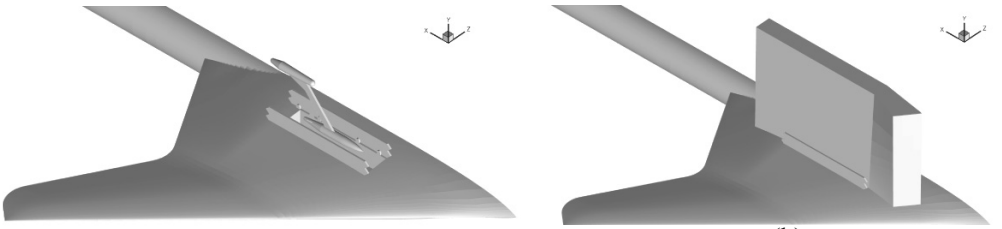
The unsteady pressure data from the four store positions are presented in Fig. 3(a). As with the previous PSD plot, offsets have been introduced for clarity. The PSD for the store at the far-field closely resembled the PSD for the M219 cavity with doors attached, where the second mode had a much higher amplitude than any other mode. The first mode was also evident and a 'bump' is visible for where the third mode should be (near 1,200Hz). Lowering the store to the centre of the doors reduced the second mode by approximately 15dB, but had little effect on the first mode or the magnitude of the broadband noise. However, the 'bump' for the third mode was no longer visible. Positioning the store on the shear layer and in the carriage locations had similar effects on the PSD. The broadband was reduced by 5-10dB and the first mode was reduced by 10dB. The amplitude of the second mode was not affected, although positioning the store in the carriage location slightly increased the frequency of the second mode.

The OASPL (Fig. 3(b)) showed that, as mentioned above, positioning the store at the shear layer and in the carriage location had similar effects and reduced the levels by 2-5dB along the bay length. The store positioned between the doors reduced the levels further, especially at the front and in the middle of the bay. Also, the reduction of the second mode changed the shape of the OASPL to a 'tick' shape, like in the M219 cavity without doors attached[7].

3.0 CFD UCAV GEOMETRY

The external geometry for the 1303 UCAV was modelled on the wind-tunnel experiments by Bruce and Mundell[14]. For the CFD computations, the geometry was non-dimensionalised by the maximum wing chord length, c. The far-field boundaries were then located at a distance of 15*c* away from the model in all three directions. Detailed explanations of the geometry and multi-block topology for the UCAV with an empty weapon bay, along with the results of computations have been presented in previous works[9-12].

https://doi.org/10.1017/S0001924000006709 Published online by Cambridge University Press



(a) (b)

Figure 4. Geometry for the UCAV with weapon bay and store (a) and surfaces of the sliding planes (b).

Figure 4(a) shows the geometry with the store placed between the doors. The extra store, sting and force balance geometry would be complex to block alone, without the added difficulty of incorporating it into the already complex UCAV-cavity blocking. Therefore. to accommodate the store, sting and force balance in the UCAV grid topology, sliding meshes were used[17]. The method involved installing surfaces into the UCAV grid that represented the sliding planes, then removing the sections of the grid inside the surfaces to create a hole, into which a second grid that encompassed the store was inserted. The sliding plane section, shown in Fig. 4(b), was able to accommodate all store positions used in the experiments[13].

The weapon bay section of the grid contained 300 cells in length, 60in width and 60in depth, which gave the cavity section a total of 1·08m cells. The removal of the sliding plane section from the original UCAV grid[12] reduced the total number of cells from 12·4m to 10·5m, while the second grid had a size of 7m points. Although this is a large increase over the original UCAV grid, it is much smaller than the grid would have been if an attempt was made to produce a multi-block structure around the whole geometry in one step.

4.0 CFD RESULTS

The governing equations are the unsteady three-dimensional compressible Navier-Stokes equations, written in dimensionless form as:

$$\frac{\partial Q}{\partial t}+\frac{\partial}{\partial x}\left(\mathbf{F}^{\mathrm{i}}+\frac{1}{\mathrm{Re}}\mathbf{F}^{\mathrm{v}}\right)+\frac{\partial}{\partial y}\left(\mathbf{G}^{\mathrm{i}}+\frac{1}{\mathrm{Re}}\mathbf{G}^{\mathrm{v}}\right)+\frac{\partial}{\partial z}\left(\mathbf{H}^{\mathrm{i}}+\frac{1}{\mathrm{Re}}\mathbf{H}^{\mathrm{v}}\right)=\vec{\mathbf{S}} \qquad \ldots (1)$$

where **F**, **G** and **H** are flux vectors and have been split into their inviscid (*i*) and viscous (*v*) parts. The source vector is denoted by $\vec{\mathbf{S}}$.

A CFD method capable of solving the compressible flow equations on multi-block structured grids using a cell-centred finite-volume method for spatial discretisation was employed in this work. A second-order implicit method[18] was employed and the resulting linear system of equations was solved using a pre-conditioned generalised conjugate gradient method. For unsteady simulations, a dual-time stepping method was employed, where the time derivative was approximated by a second-order backward difference based on Jameson's pseudo-time integration approach[19]. The resulting nonlinear system of equations was solved by integration in pseudo-time using first-order backward differences. In each pseudo-time step, a linearisation is used to obtain a system of equations that is solved using a generalised conjugate gradient method with a block-incomplete lower-upper pre-conditioner. From the beginning, the solver was designed with parallel execution in mind and for this reason a divide-and-conquer approach was used to allow for multi-block grids to be computed on distributed-memory machines and especially on low-cost

https://doi.org/10.1017/S0001924000006709 Published online by Cambridge University Press

Beowulf clusters of personal computers. Variants of this method for many aerospace applications have been published[5,20-23].

For the discretisation of the convective fluxes, Osher's upwind scheme[24] has been used and a formally third-order accurate scheme is achieved using a MUSCL variable extrapolation technique. Viscous fluxes are discretised using central differences. Boundary conditions are set using two layers of halo cells. The final system of algebraic equations is solved using a preconditioned Krylov subspace method. The computations presented here employed the DES.with the S–A turbulence model[25].

The simulation was performed at a Mach number of 0·85; however, the added complexity from the addition of the store, sting and force balance meant that achieving a grid of high enough quality for a high Reynolds number computation was difficult. This was also problematic due to the inaccuracy of the initial CAD model. Therefore, it was decided to reduce the Reynolds number down from the experimental value of approximately seven million to one million for this configuration. Previous cavity flow simulations have shown that a simular reduction in Reynolds number has a small effect on the cavity flow-field[5], and resulted in substantial savings in CPU time.

The large size of the mesh and the use of the sliding mesh method made this an expensive case to compute. The computation used approximately 74,000 CPU hours and included 8,200 steps. After discarding an initial part of the transient data, the signal length was approximately 0·01 seconds, equivalent to about three periods of the lowest Rossiter mode. Although this is a short signal length, it can be analysed to provide an idea of the accuracy compared to the experiments. Note that mesh size and density was based on past experience with the cavity flow problem and so no deliberate attempt was made to optimise the mesh size or sliding plane. Also, since the experimental data were limited to unsteady pressure data, a thorough comparison of DES flowfield with experiments was not possible.

4.1 Unsteady pressure data

Figure 5 shows the PSD on the bay floor near the aft wall for the UCAV with an empty weapon bay and with the store between the doors. For both cases, the largest tone occurs at a frequency slightly higher than the prediction of the second Rossiter mode, which is consistent with the experimental data. For the empty UCAV bay, there is a slight peak around the first mode but no tones can be seen above the broadband level for the third or fourth modes. In comparison to the experimental data, the frequencies and magnitudes of the first two tones were predicted well. The peak level of the second mode was within 2dB of the experimental data at all locations along the bay floor. For the store case, the signal was not really long enough to resolve the higher frequency, more intermittent modes. Even so, the general levels of the SPL were predicted well.

The overall sound-pressure level (OASPL) across the bay floor was also computed and is shown in Fig. 6. As the experimental data was shortened to the numerical signal length, the minimum and maximum fluctuations in the full signal are represented by the error bars. These fluctuations were computed by splitting the experimental signal up into sections of length equal to the numerical data, with the sections also having a 90% overlap. The OASPL was then computed for each section of the maximum and minimum values found. A small overprediction in the OASPL can be seen all along the bay floor and has a maximum of 3dB for the empty bay and 5dB for the store case. This is consistent with other computations for idealised cavity flows, where over-predictions as high as 5dB are reported[7]. The error bars on Fig. 6(a) show fluctuations in the experimental data are as high as 5dB for the empty bay. The fluctuations in the experimental values are larger for the store case due to the short signal length in the CFD results. These comparisons were very encouraging, especially for such a complex geometry.

https://doi.org/10.1017/S0001924000006709 Published online by Cambridge University Press

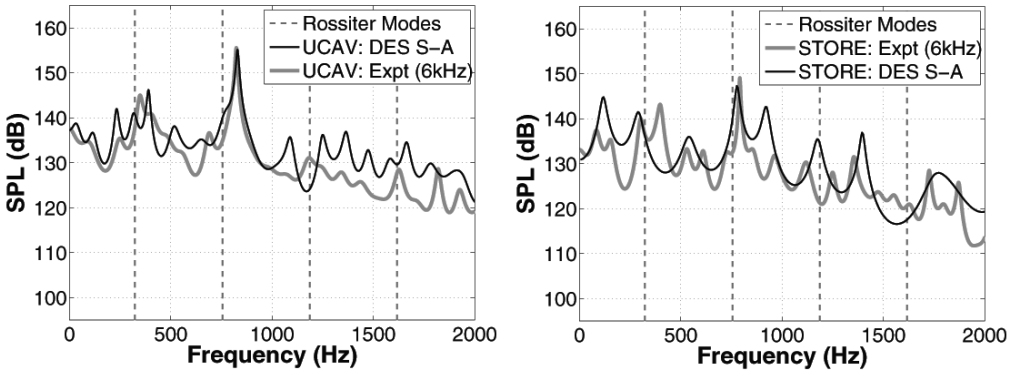


Figure 5. PSD plots at x/L = 0·92 for the UCAV with empty weapon bay and with a store between the doors comparing results from computations to the experimental data from Hill and Lawson[13]. PSD Plots are presented in terms of SPL and vertical dashed lines on PSD represent the frequencies of Rossiter's modes[3].

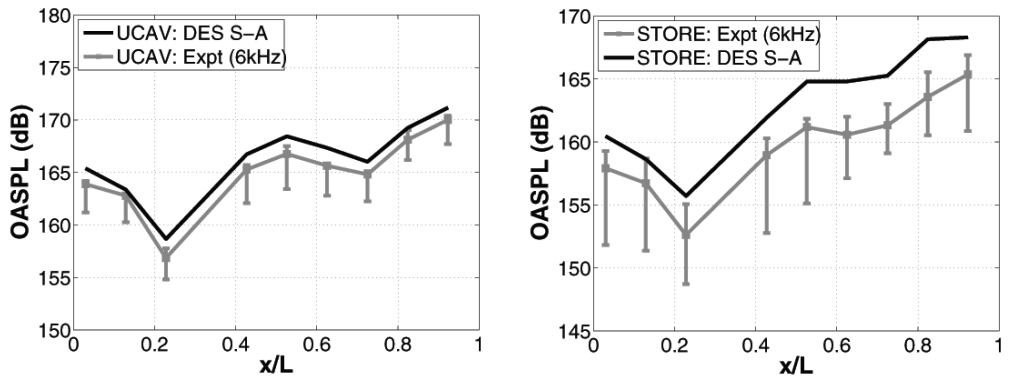


Figure 6. OASPL for the UCAV with empty weapon bay and with a store between the doors comparing results from computations to the experimental data from Hill and Lawson[13].

4.2 Flow-field comparisons

Figure 7 shows iso-surfaces of Q-criteria[26]. This quantity is frequently used instead of vorticity, for the visualisation of unsteady turbulent flows and highlights the shape and size of the vortical structures present at each time instance. Here, the vortical flow emanating from the centre of the doors and the door hinges is visible. In addition, small structures are present inside the cavity originating from the rear end and the fins of the store. Structures were also seen at the point where the sting attaches to the store. The sting and force balance had a strong effect on the flow and vortex shedding was observed from the blunt trailing edge of the sting and the rear of the force balance.

The addition of the store in between the doors had a major effect in reducing the oscillations of the shear layer. The boundary layer separated from the UCAV at the leading edge of the cavity as in the empty cavity case; however, the store appeared to restrict the motion of the shear layer above the cavity opening. Downstream of the store apex, the blockage induced by the store deflected the shear layer down into the cavity. After the mid-point, the reduced thickness allowed the shear layer to oscillate, although at a much reduced level than in the empty cavity configuration.

Averaged flow-fields are shown in Figs 8 and 9. The short length of the store computation meant that only 36 flow realisations over a time period of $8{\cdot}5\times10^{-3}$ seconds were used to create

https://doi.org/10.1017/S0001924000006709 Published online by Cambridge University Press

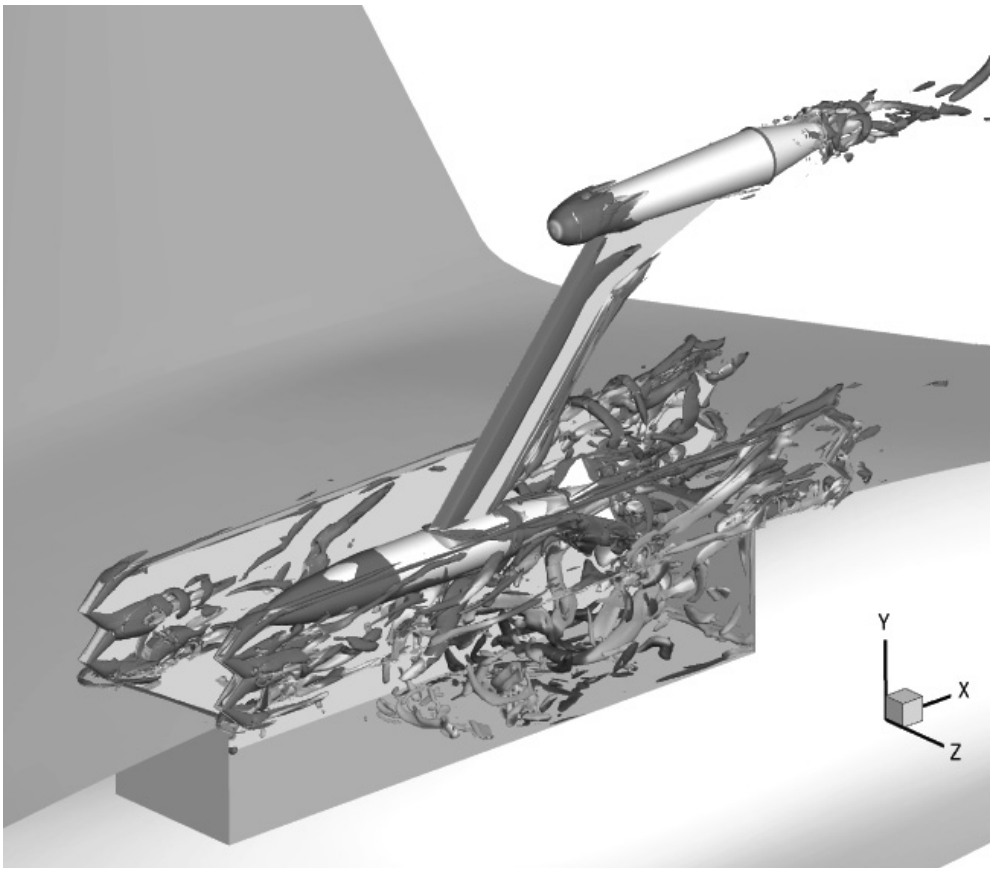


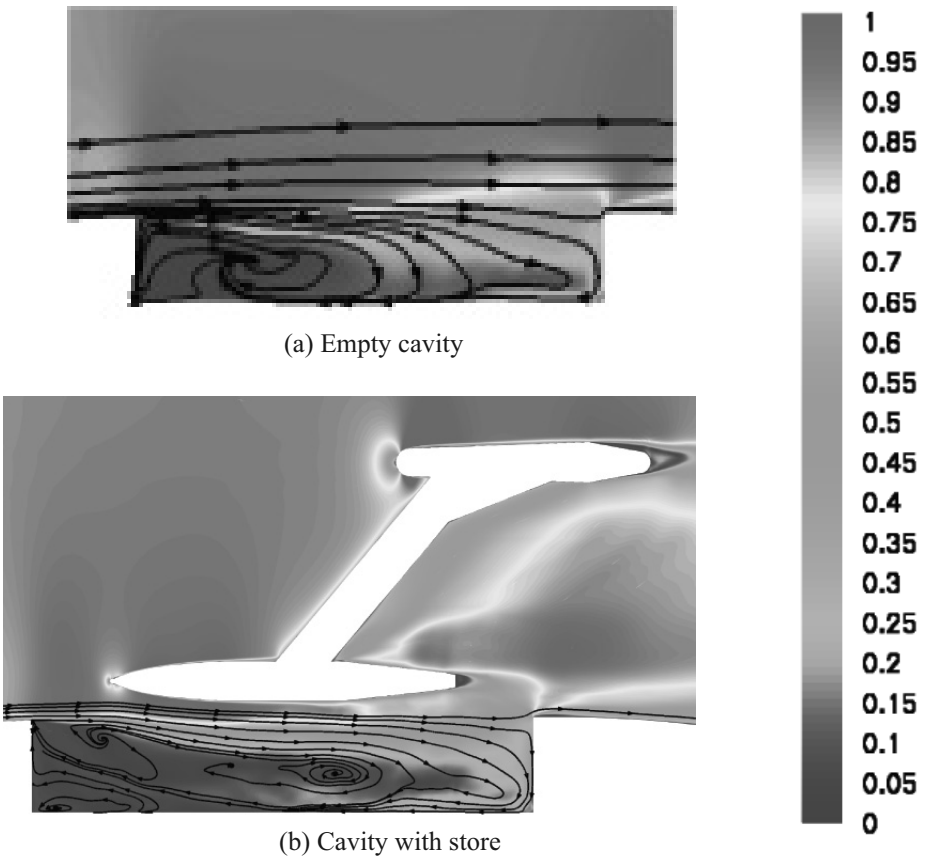
Figure 7. Instantaneous iso-surfaces of Q-Criteria for the UCAV weapon bay with a store between the doors. Iso-surfaces at Q = 2,000 are shown and coloured with streamwise velocity (non-dimensionalised with respect to the free-stream velocity), where levels are between –0·5 (blue) and +0·5 (red).

the averaged flow-field (compared to 101 over a time period of $3{\cdot}1\times10^{-2}$ seconds for the empty cavity). This was simply due to the limited amount of CPU time available for this investigation. Even so, the general characteristics of the flow can be identified from the averaged data.

The large oscillations of the shear layer in the empty cavity caused the centre of the primary vortex to be located in the front half of the cavity, rather than in the rear. This allowed the shear layer to stay coherent into the cavity to a much higher degree than in the M219 cavity configuration. Figure 8(b) also shows the flow above Mach 1 over the upper surface over the UCAV and a weak shock, which was located at approximately x/c local of 0·6 as in the baseline configuration.

In the store configuration, the centre of the primary vortex was located at slightly past the mid-point of the cavity. There was also a vortex in the front lower corner of the cavity, which was larger than the ones observed in the M219 cavity configurations. Figure 9 also shows that the small recirculation bubbles observed for the M219 clean cavities were also present for both UCAV cases. The views of the cavity leading and trailing edges show another irregularity of this cavity, where the trailing edge corner was lower than the leading edge. The stagnation streamline for both configurations attaches to the wall at an upward angle, with the location also very similar.

https://doi.org/10.1017/S0001924000006709 Published online by Cambridge University Press



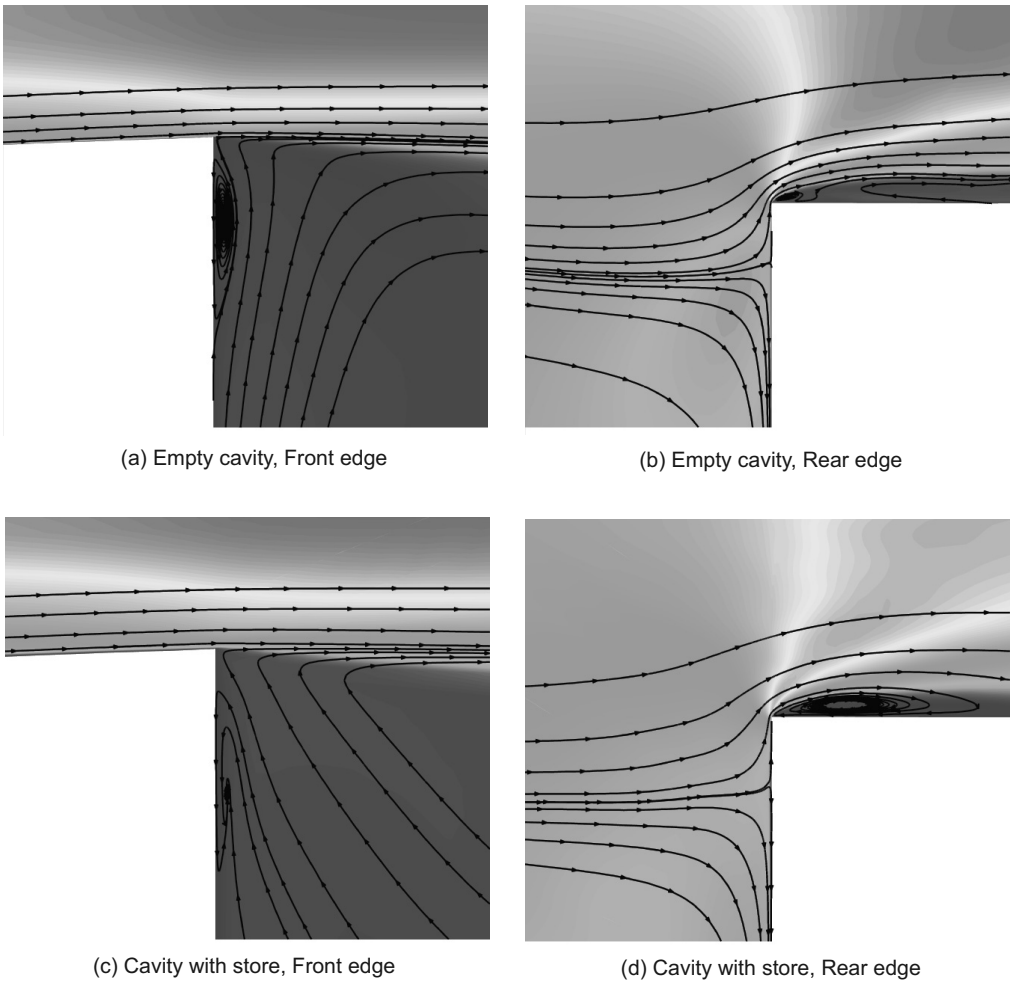
(a) Empty cavity

(b) Cavity with store

Figure 8. Averaged contours of Mach number for the empty UCAV cavity (a) and with a store between the doors (b). Streamlines are also shown to identify the general flow structure. Planes are located at the cavity centreline.

Although averaged plots in the streamwise direction show the influence of the store on the cavity dynamics, the influence in the spanwise direction is not as great. Instantaneous contours of Mach number show that the position of the store has little direct influence on the store regarding its interaction with the shear layer, although the presence of the store still resulted in reduced oscillations within the cavity. Even with the large differences in the instantaneous flow-fields the averaged flow-fields were much more similar. Figure 10 shows averaged contours at $x/L = 0{\cdot}2$, $0{\cdot}5$ and $0{\cdot}8$. Note that the UCAV with an empty cavity was averaged over a longer duration than the configuration with the store and for this reason asymmetries for the UCAV with store case are more pronounced. At all locations, the averaged flow on either side of the bay (such as the vortices created on the outside of the doors, the boundary layer on the UCAV surface and on the tops of the doors) is similar for both configurations. At $x/L = 0{\cdot}2$, the vortices on the inside of the doors were more defined for the store configuration. The profile of the shear layer is, however, similar for both cases. At the second location, the Mach number above the store is lower since the position of the slice is just in front of the sting supporting the store. Again, the profile of the shear layer is similar to the empty UCAV configuration; however, the reduced averaging period for the store configuration is evident inside the cavity. At the final location, the fins on the store and a section of the sting supporting

https://doi.org/10.1017/S0001924000006709 Published online by Cambridge University Press



(a) Empty cavity, Front edge

(b) Empty cavity, Rear edge

(c) Cavity with store, Front edge

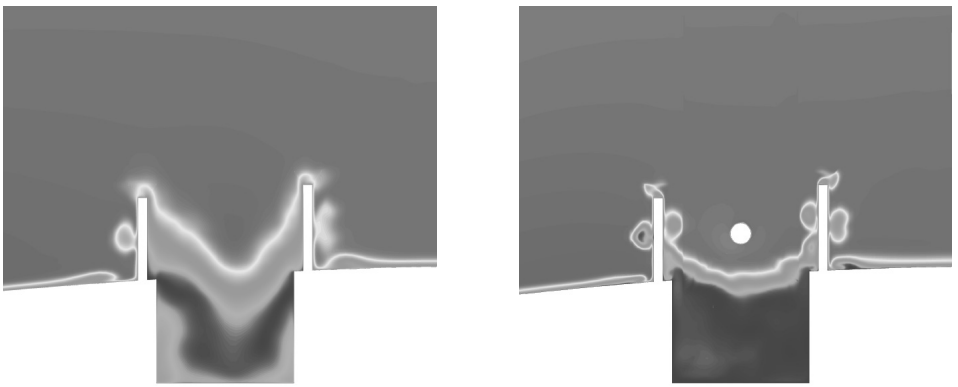
(d) Cavity with store, Rear edge

Figure 9. Averaged contours of Mach number at the cavity leading and trailing edges for the empty UCAV cavity (a,b) and with a store between the doors (c,d). Streamlines are also shown to identify the general flow structure. Plane is located at the cavity centreline.

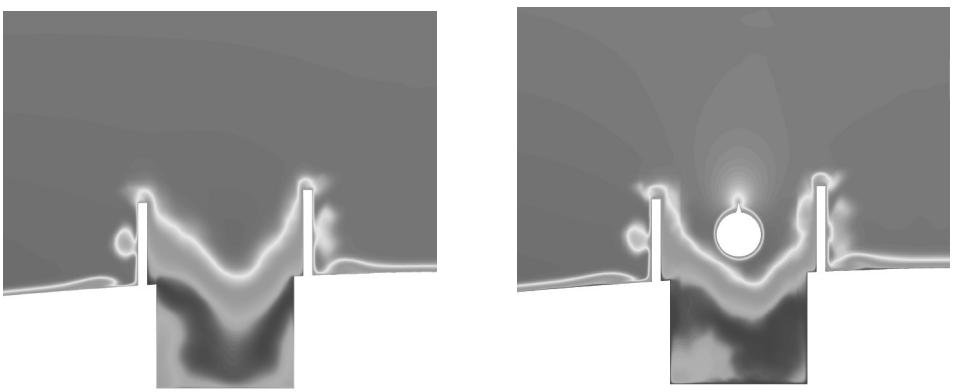
the store are visible. Although not shown in the plot, the force balance is above the section of the sting and so areas of high Mach number are visible on either side of the sting.

The pitch and yaw flow angles around the weapon bay are shown in Figs 11 to 14. The averaged pitch angles shows a concentration of activity inside the cavity with values near zero between the doors and above the shear layer. Inside the cavity, the presence of a vortex in the averaged flow is evident for the stations x/L=0·1 and 0·5, with the sign of the angle values changing from positive to negative. The last station at x/L = 0·9 shows a more irregular pattern as expected due to the presence of finer structures, as visualised with the Q-Criteria in Fig. 7. The peak to peak values of Fig. 12 are very similar between the empty bay and with a store. As can be seen, the store is located above the shear layer, while most of the activity is concentrated inside the weapon bay. In itself, this is a positive result, suggesting that once the store has cleared the shear layer, its trajectory may not be influenced by the cavity anymore.

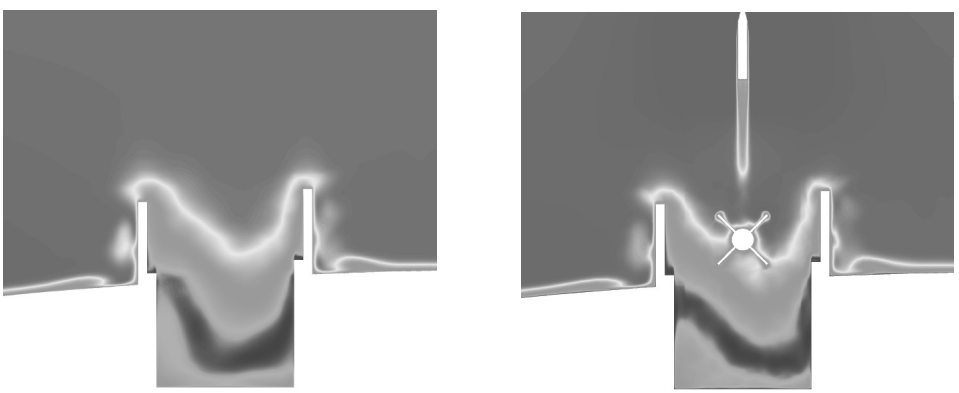
https://doi.org/10.1017/S0001924000006709 Published online by Cambridge University Press



(a) x/L = 0·2



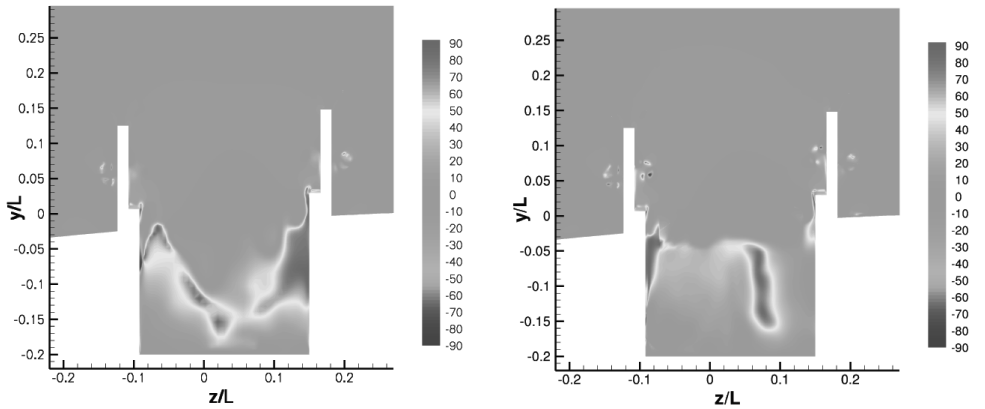
(b) x/L = 0·5



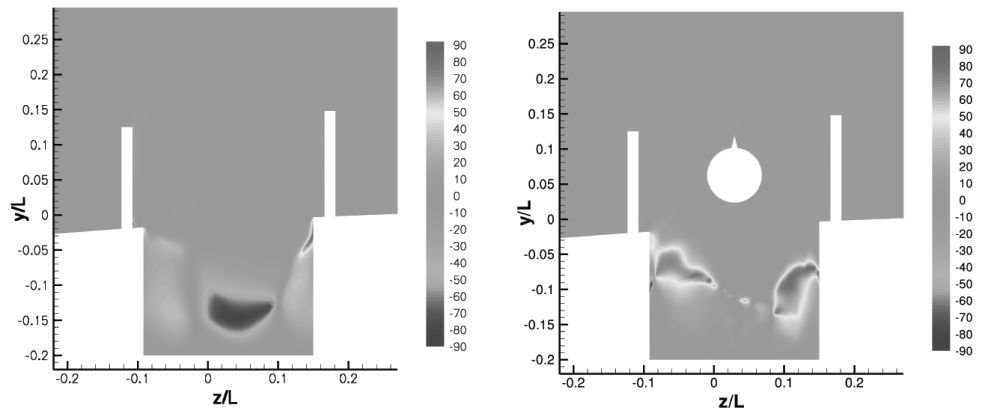
(c) x/L = 0·8

Figure 10. Averaged contours of Mach number for the empty UCAV cavity (left column) and with a store between the doors (right column). Mach number levels range between 0 (blue) and 1 (red).

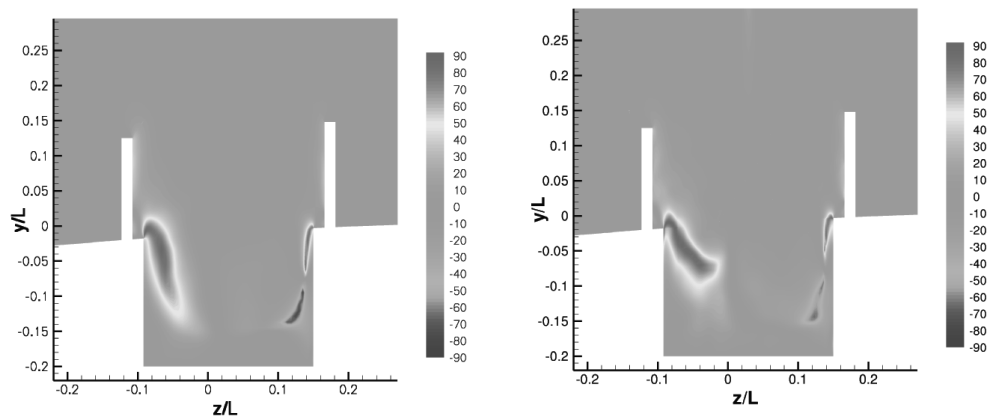
https://doi.org/10.1017/S0001924000006709 Published online by Cambridge University Press



(a) x/L = 0·1



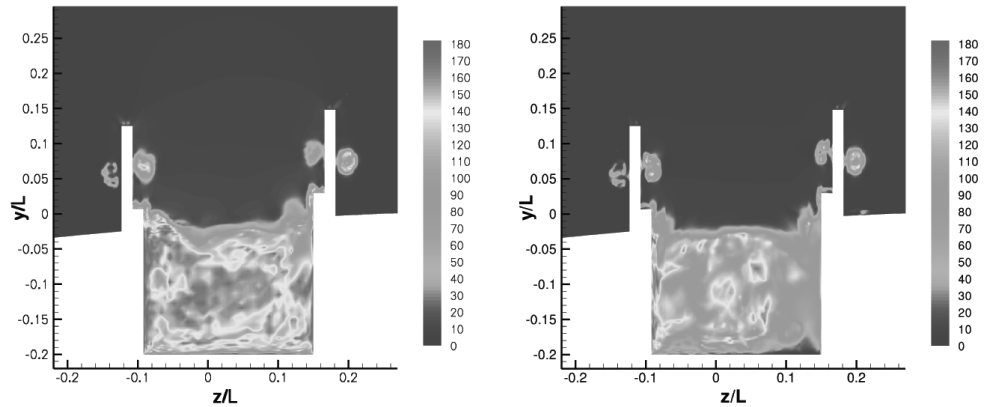
(b) x/L = 0·5



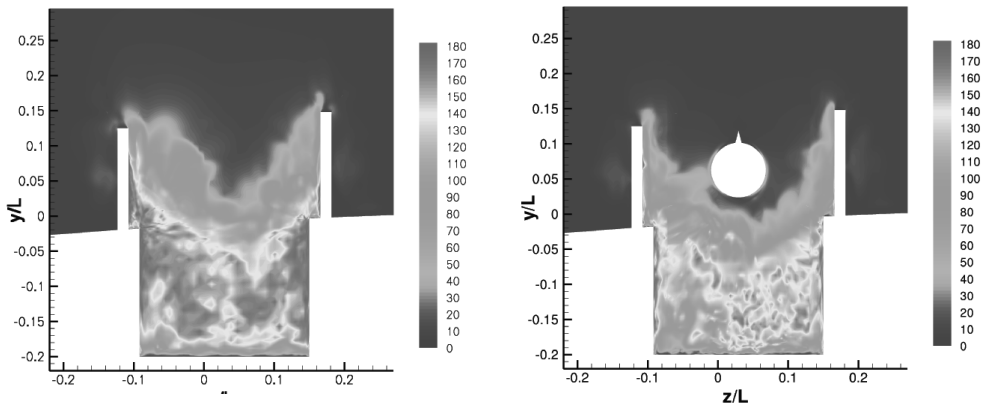
(c) x/L = 0·9

Figure 11. Contours of averaged pitch flow angles for the empty UCAV cavity (left column) and with a store in between the doors (right column).

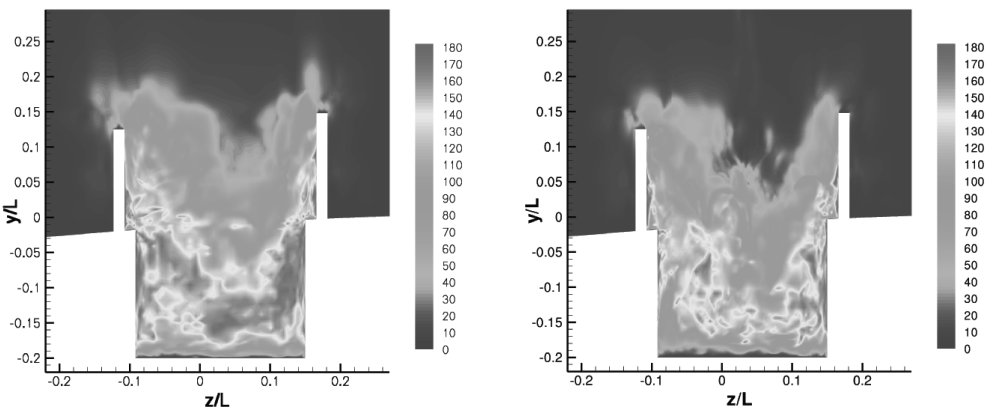
https://doi.org/10.1017/S0001924000006709 Published online by Cambridge University Press



(a) $x/L = 0{\cdot}1$



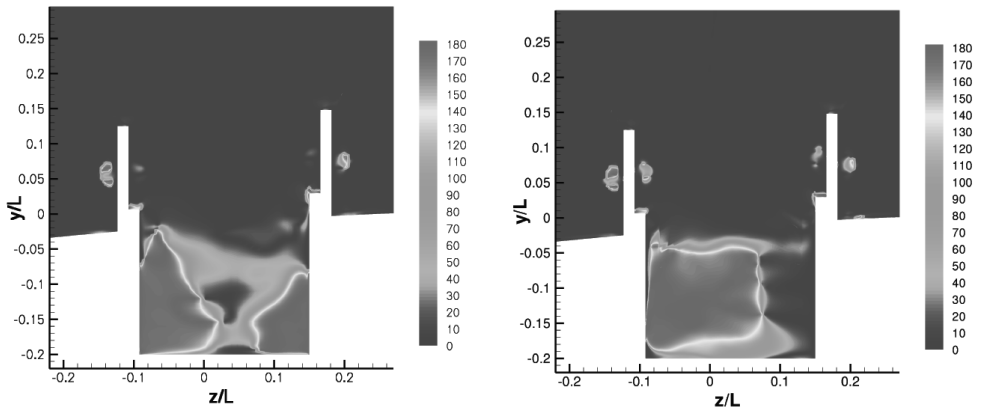
(b) $x/L = 0{\cdot}5$



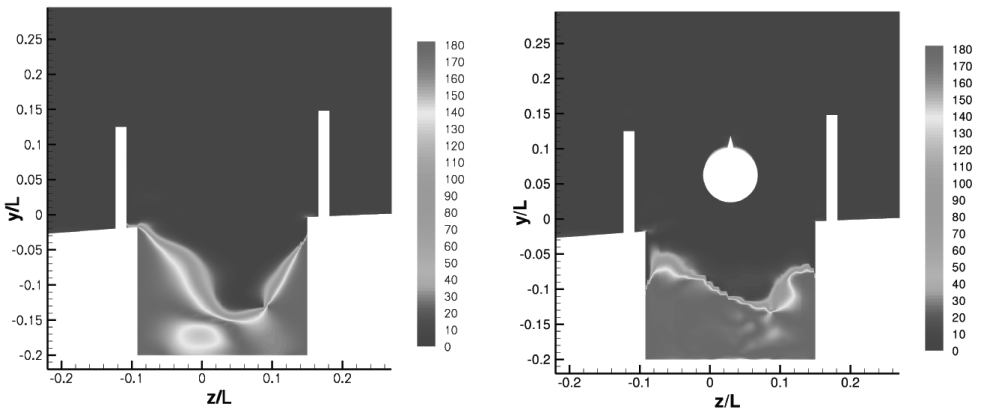
(c) $x/L = 0{\cdot}9$

Figure 12. Contours of peak to peak pitch flow angles for the empty UCAV cavity (left column) and with a store in between the doors (right column).

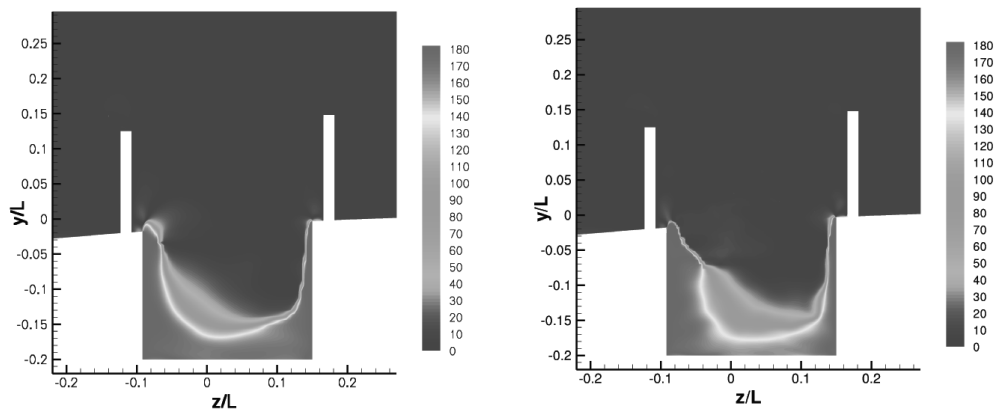
https://doi.org/10.1017/S0001924000006709 Published online by Cambridge University Press



(a) x/L = 0·1



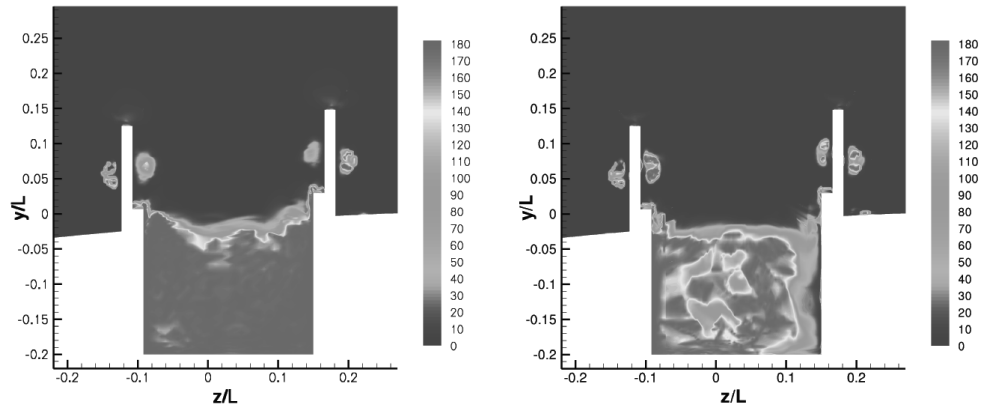
(b) x/L = 0·5



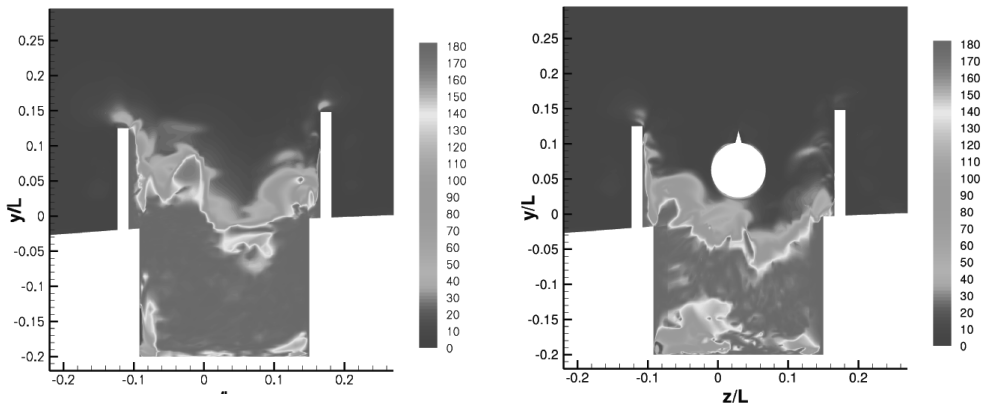
(c) x/L = 0·9

Figure 13. Contours of averaged yaw flow angles for the empty UCAV cavity (left column) and with a store in between the doors (right column).

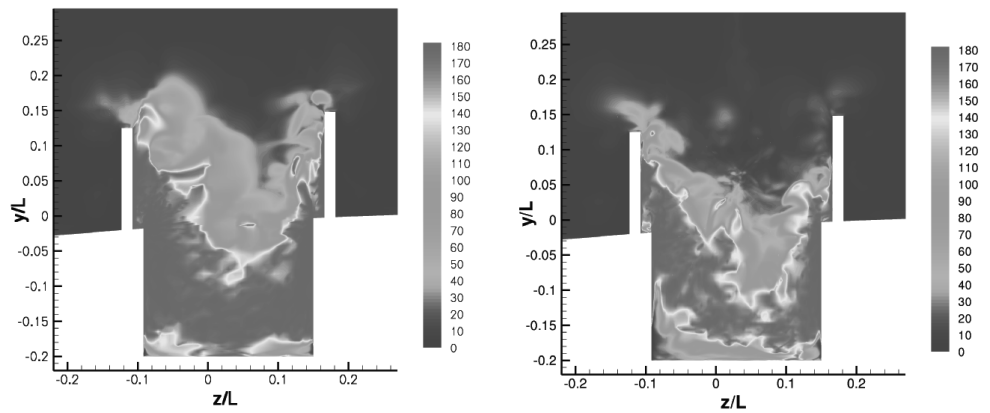
https://doi.org/10.1017/S0001924000006709 Published online by Cambridge University Press



(a) x/L = 0·1



(b) x/L = 0·5



(c) x/L = 0·9

Figure 14. Contours of peak to peak yaw flow angles for the empty UCAV cavity (left column) and with a store in between the doors (right column).

https://doi.org/10.1017/S0001924000006709 Published online by Cambridge University Press

The same remarks can be made for the yaw angle plots shown in Figs 13 and 14. The flow clearly changes direction close to station $x/L = 0{\cdot}9$ in the middle of the cavity. The flow near the cavity walls appears to have the same direction since the flow is restricted by the walls. The last station shows remarkable similarity between the two test cases. Most of these are apparently due to the asymmetric shape of the weapon bay. For all cases, the doors appear to confine the flow in the spanwise direction as was the case for the idealised M219 cavity.

The peak to peak values appear similar between the two cases with only the $x/L = 0{\cdot}5$ station showing some interaction between the store and the shear layer. Clearly the store pushes the flow further towards the cavity, although the overall structure of the contours remains unchanged. Again, the rear of the cavity is very similar, especially for the region below the shear layer. Somehow lower values of the peak to peak changes appear in the region behind the store. This was expected since the store itself shields the flow behind it from the energetic free-stream. Consequently, low values are encountered between the doors.

A PIV study would be a good addition to this experiment and could help reinforce the conclusions from the CFD results.

5.0 CONCLUSIONS

For the computations of the full UCAV configuration, advanced multi-block topologies had to be used to properly represent the planform of the UCAV and all the details of the cavity, including doors and hinges, while sliding meshes were needed to insert the store. Computations with an empty cavity and with a store between the doors were carried out using the DES S-A model and comparisons to experimental data were very encouraging for such complex configurations. Visualisations using the Q-criteria revealed the added turbulent content due to the door leading edges and the door hinges. For the empty cavity, the primary vortex was located in the front part of the cavity and this reduced the fluctuating components of the velocities to lower values than in the idealised M219 case. The addition of a store in between the doors had little effect close to the front wall. However averaged flow-fields showed that the proximity of the shear layer to the apex of the store deflected it into the cavity and restricted its growth. Further downstream, the influence of the store reduced and the shear layer thickened at a rate higher than for the empty case. Outside the cavity, additional vortex shedding was observed from the sting and force balance. Given the short length of the signal obtained for the UCAV store configuration, the agreement with the experimental data is remarkably good for the OASPL as well as the frequencies of the tones present.

ACKNOWLEDGEMENTS

The financial support of EPSRC through grant EP/C533380/1 is gratefully acknowledged. The authors would like to thank Trevor Birch of DSTL for the experimental data and the UK 2nd Applied Aerodynamics Consortium for the use of HECToR.

REFERENCES

1. ROSHKO, A. Some measurements of flow in a rectangular cut-out, August 1955, Technical report, NACA Technical Report 3488, California Institute of Technology.
2. KRISHNAMURTY, K. Acoustic radiation from two-dimensional rectangular cutouts in aerodynamic surfaces, , August 1955, Technical Report Technical Note 3487, National Advisor Committee For Aeronautics.

https://doi.org/10.1017/S0001924000006709 Published online by Cambridge University Press

3. ROSSITER, J.E. Wind tunnel experiments on the flow over rectangular cavities at subsonic and transonic speeds, October 1964, Technical Report 64037, Royal Aircraft Establishment.
4. LARCHEVÊQUE, L., SAGAUT, P., LÊ, T.-H and COMTE, P. Large-eddy simulation of a compressible flow in a three-dimensional open cavity at high Reynolds number, *J Fluid Mechanics*, 2004, **516**, pp 265–301.
5. NAYYAR, P., BARAKOS, G.N. and BADCOCK, K.J. Numerical study of transonic cavity flows using large-eddy and detached-eddy simulation, *Aeronaut J*, 2007, **111**, (1117), pp 153–164.
6. BARAKOS, G.N., LAWSON, S.J., STEIJL, R. and NAYYAR, P. Numerical simulations of high-speed turbulent cavity flows, *Flow, Turbulence and Combustion*, December 2009, **83**, (4), pp 569–585, doi:10.1007/s10494-009-9207-1.
7. LAWSON, S.J. and BARAKOS, G.N. Assessment of passive flow control devices for transonic cavity flows using detached-eddy simulation, *J Aircr*, May-June 2009, **46**, (3), pp 1009–1029, doi:10.2514/1.39894.
8. WONG, M.D., MCKENZIE, G.J., OL, M.V., PETTERSON, K. and ZHANG, S. Joint TTCP CFD studies into the 1303 UCAV performance: First year results, 2006, AIAA-2006- 2984, 24th AIAA Applied Aerodynamic Conference, San Francisco, CA, USA, 5-8 June 2006.
9. LAWSON, S.J. and BARAKOS, G.N. DES for UCAV weapon bay flow, 2009, Third Symposium on Hybrid RANS-LES Methods, 10-12 June 2009, Gdansk, Poland.
10. LAWSON, S.J. and BARAKOS, G.N. Evaluation of DES for flows around UCAVs, 2009, Paper 3572, CEAS 2009 European Air and Space Conference, 26-29 October 2009, Manchester, UK.
11. LAWSON, S.J. and BARAKOS, G.N. Evaluation of DES for weapons bays in UCAVs, 2010, AIAA-2010-1425, 48th Aerospace Sciences Meeting, 4-7 January 2010, Orlando, FL, USA.
12. LAWSON, S.J. and BARAKOS, G.N. Evaluation of DES for weapons bays in UCAVs, *Aerospace Sci and Tech*, 2010, (article in press), doi: 10.1016/j.ast.2010.04.006.
13. HILL, A.C. and LAWSON, S.G. Tests conducted in the ARA 2·74m × 2·44m transonic wind tunnel on the release of a generic MK82/GBU-30 JDAM store model from a generic UCAV model using the ARA two sting rig, November, 2004, Technical Report, ARA.
14. BRUCE, R.J. and MUNDELL, A.R.G. Low speed wind tunnel tests on the 1303 UCAV concept, March 2003, Technical Report QINETIQ/FST/TR025502/1.0, QinetiQ, Farnborough, UK.
15. BRUCE, R.J. High speed wind tunnel tests on the 1303 UCAV concept, June 2003, Technical Report QINETIQ/FST/TR030214/1.0, QinetiQ, Farnborough, UK.
16. NIGHTINGALE, D.A., ROSS, J.A. and FOSTER, G.W. Cavity unsteady pressure measurements — Examples from wind-tunnel tests, November 2005, Technical Report Version 3, Aerodynamics & Aeromechanics Systems Group, QinetiQ.
17. STEIJL, R. and BARAKOS, G.N. Sliding mesh algorithm for CFD analysis of helicopter rotor-fuselage aerodynamics, *Int J for Numerical Methods in Fluids*, October 2008, **58**, (5), pp 527–549, doi:10.1002/fld.1757.
18. STEIJL, R., BARAKOS, G. and BADCOCK, K. A framework for CFD analysis of helicopter rotors in hover and Forward flight. *Int J Numerical Methods in Fluids*, 2006, **51**, (8), pp 819–847, doi:10.1002/fld.1086.
19. JAMESON, A. Computational algorithms for aerodynamic analysis and design, Applied Numerical Mathematics, 13(5):383–422, 1993.
20. BADCOCK, K.J., RICHARDS, B.E. and WOODGATE, M.A. Elements of computational fluid dynamics on block structured grids using implicit solvers, *Progress in Aerospace Sciences*, 36, (5-6), pp 351–392, July 2000.
21. MORVANT, R., BADCOCK, K.J., BARAKOS, G.N. and RICHARDS, B.E. Aerofoil-vortex interaction using the compressible vorticity confinement method. *AIAA J*, January 2005, **43**, (1), pp 63–75.
22. SPENTZOS, A., BARAKOS, G.N., BADCOCK, K.J., RICHARDS, B.E., WENERT, P., SCHRECK, S. and RAFFEL, M. Investigation of three-dimensional dynamic stall using computational fluid dynamics, *AIAA J*, May 2005, **43**, (5), pp 1023–1033.
23. BARAKOS, G.N., STEIJL, R., BADCOCK, K.J. and BROCKLEHURST, A. Development of CFD capability for full helicopter engineering analysis, 2005, 31st European Rotorcraft Forum, September 2005, Florence, Italy.
24. OSHER, S. and CHAKRAVARTHY, S. Upwind schemes and boundary conditions with applications to Euler equations in general geometries, *J Computational Physics*, 1983, **50**, pp 447–481.
25. SPALART, P.R., JOU, W-H., STRELETS, M. and ALLMARAS, S.R. Comments on the feasibility of LES for wings and on a hybrid RANS/LES approach, 1997, 1st AFOSR International Conference on DNS/LES, Columbus, OH, USA, 4-8 August 1997.
26. JEONG, J. and HUSSAIN, F. On the identification of a vortex, *J Fluid Mech*, 1995, **285**, pp 69–94.

https://doi.org/10.1017/S0001924000006709 Published online by Cambridge University Press